

# Mooring system fatigue analysis for CALM and SALM oil terminals

Esmaeil Hasanvand<sup>1</sup>, Pedram Edalat<sup>2\*</sup>

<sup>1</sup> M.Sc. Offshore Structure Engineering Department, Petroleum University of Technology, E.hasanvand@mnc.put.ac.ir

<sup>2</sup> Assistant Professor, Mechanical Engineering Department, Petroleum University of Technology, Edalat@put.ac.ir

## ARTICLE INFO ABSTRACT

Article History:  
Received: 18 Feb. 2021  
Accepted: 27 Jun. 2021

**Keywords:**  
Mooring system  
Fatigue analysis  
T-N curve  
Oil terminal  
OrcaFlex

Offshore oil terminals are a cheaper and safer solution than conventional shore terminals for unloading and loading tankers. There are several types of offshore terminals, including Catenary Anchor Leg Mooring (CALM) and Single Anchor Leg Mooring (SALM). Safety is crucially important for offshore terminals. However, over the past few decades, mooring accidents of permanent floating structures have occurred quite frequently in the last few decades. Most of these failures have been caused by fatigue load. T-N curves-based mooring system fatigue analyses for a CALM and SALM oil terminal are presented. Stress amplitudes are calculated based on the tension amplitudes of the mooring lines under the combined loading process due to wave frequency (WF) and low frequency (LF) motion. A comparison is made between CALM and SALM mooring fatigue designs based on the conditions of the Persian Gulf region. For simulation, the hydrodynamic response characteristics of terminals and tankers are first calculated using ANSYS AQWA software, and then the outputs are imported into ORCAFLEX software for fatigue analysis. The results show that under the same environmental conditions with the same tanker tonnage, the SALM terminal mooring system shows a greater fatigue life. The minimum fatigue life of the mooring system for CALM and SALM terminals occurs at near the touch-down position (TDP) and the near of connection to the seabed, respectively. It is revealed that by changing the value of minimum breaking strength (MBS) the fatigue life of the CALM and SALM terminals changes by 119% and 100%, respectively. It is also observed that by changing the amount of  $K$  value (the value for platted T-N curve), the fatigue life of the CALM and SALM terminals changes by the same amount. In all cases, the value of  $R$  (the ratio of tension range to reference breaking strength), in the mooring line of SALM terminal, although more tension is generated, the ratio of  $R$  is less and will improve the life of fatigue.

## 1. Introduction

One of the most important requirements and challenges in the oil industry is the safe transfer of oil products. Petroleum products are generally transported through offshore pipelines and oil terminals (using shuttle tankers). Oil terminals are divided into shore and offshore categories. In shore terminals, when the environmental conditions are favorable, the tankers are moored on the shore, and after they are placed at the site, loading and unloading operations are performed. In offshore terminals, petroleum products are transported via pipelines to safer offshore areas and after the tanker is moored by floating terminals, it is loaded. Therefore, no complex mooring operation is performed in this case compared to the shore terminals. The tendency to use offshore terminals has increased due to the high cost of installation, long construction time, maintenance requirements, including dredging, on the one hand, and the risks of unloading and loading operations of shore terminal.

One of the most important tasks of offshore terminals is to ensure the supply of a safe site for the tanker to be moored. As such, the pipes and risers connected to it will not be damaged. So, since the control of movements in these terminals is the responsibility of the mooring system, the mooring system has a key role in maintaining the position of the tanker in connection with the terminal. Therefore, recognizing the effective parameters in these systems will lead to further understanding of the strengths and weaknesses of these oil terminals.

Offshore oil terminals have different types depending on how the tanker is controlled and how petroleum products are transported. But, two of them, including CALM and SALM, are more common than the others. A schematic of them is presented in Figure 1.

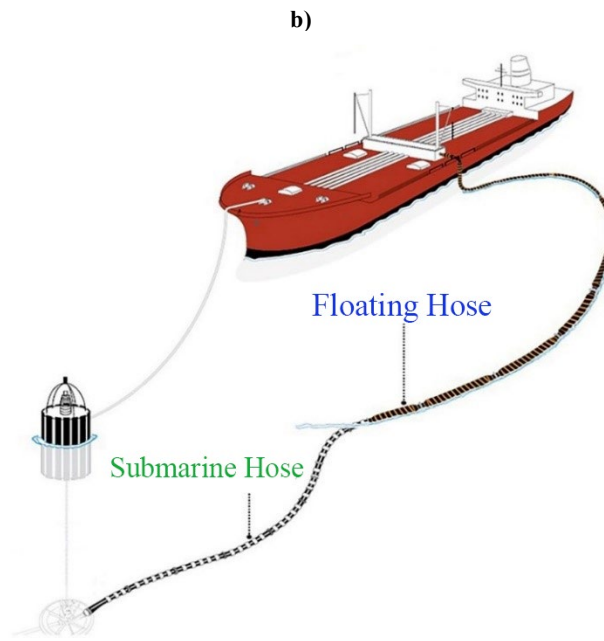
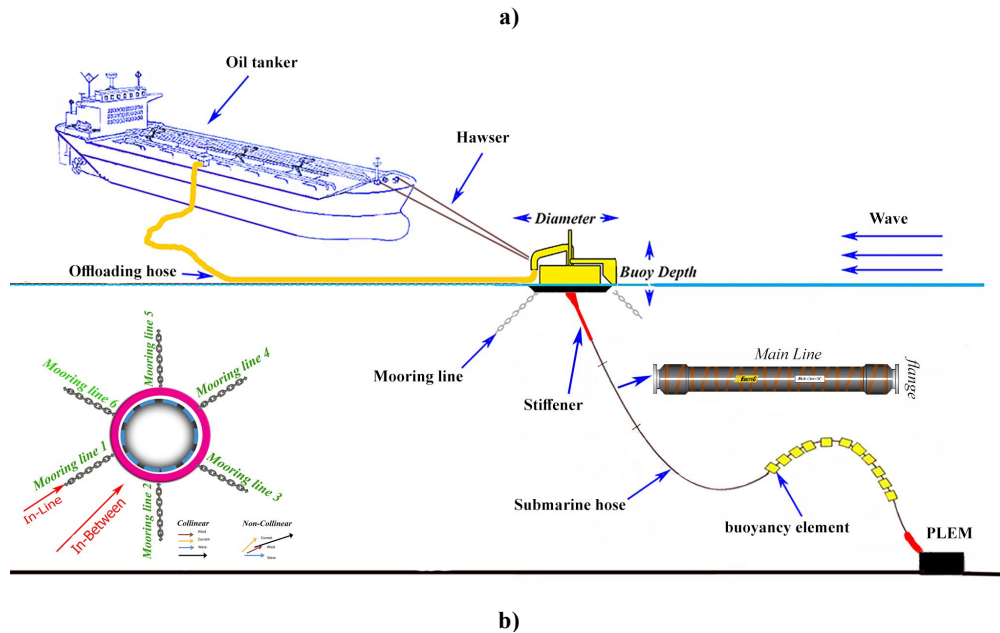


Figure 1: A schematic view of two common types of offshore oil terminals including a) CALM terminals and, b) SALM terminals

The use of CALM terminals, which are the most commonly used terminals for the transfer of oil products, has been started since 1959. A CALM terminal consists of a cylindrical buoy that is connected to the seabed by four to six mooring lines. This structure itself is also the most common type of terminal. This buoy consists of two parts – an upper part and a lower part. The lower part is in the water, and the buoyant force is applied to it and it is fixed to the seabed by a mooring system. The upper part is connected to the lower part by a bearing and allows 360-degree rotation. The tanker is connected to the upper part of the buoy by a hawser, which allows the tanker to rotate. The petroleum products enter the floating buoy of the terminal through a riser and are transferred from the buoy to the tanker by flexible floating pipes[1].

SALM terminals were first used in 1969, and after CALM, they are most widely used in the transport of petroleum products from the seabed to tankers in offshore operations. The SALM structure, as shown in

Figure 1-b, is connected to the seabed only by one mooring line, and unlike the previous structure in which petroleum products are transported first from the seabed to the terminal and then to the tanker, in this case, the products are directly transported from the seabed to the tanker[2].

Safety is crucially important for offshore terminals. However, over the past few decades, mooring accidents of permanent floating structures have occurred quite frequently in the last few decades. Most of these failures have been caused by fatigue load. Due to the cyclic loadings in offshore areas, including waves, the fatigue analysis of mooring systems of these terminals is of special importance[3]. Estimating the life of these structures in the same operating and environmental conditions can contribute to selecting an appropriate oil terminal. Therefore, there is a need to develop reliable methods to assess the fatigue of mooring systems at the design stage.

Recently, there have been some attempts to do fatigue and dynamic analysis on mooring systems. de Laval

(1971) attempted to understand the fatigue behavior of offshore mooring chains in a series of fatigue tests on mooring chains[4]. Xue et al (2018) compared S-N curves, T-N curves, and fracture mechanics (FM) for mooring fatigue analyses in the semi-submersible platform. Their results showed that if the safety factors proposed by API and DNVGL were considered in the T-N and S-N curve approaches, the fatigue life predicted by the three methods would be comparable. The results also showed that the fatigue life of a mooring chain predicted by the FM approach was generally sensitive to the initial crack shape and initial crack sizes, but it was not relatively sensitive to the critical crack depth. The T-N curve approach to predict the fatigue life of a chain was found to be slightly more conservative than the S-N curve approach[3]. Olsen (2018) investigated the probability of the failure of a mooring system of a semi-submerged structure with 14 mooring chains as a function of safety coefficients based on different standards. This study used laboratory results and then the results extracted from SIMO software to assess the probability of failure. Finally, the results of the two models were compared. It was revealed that the probability of mooring failure due to the maximum force obtained by SIMO was significantly lower than the results of the laboratory model[5]. Wu et al. (2015) performed an analytical analysis for the low frequency (LF) and wave frequency (WF) fatigue analysis according to the T-N curve approach along a catenary mooring line with homogeneous materials. The most significant LF fatigue damage was found to occur at the bottom of a mooring line near the touch position. For WF fatigue, several factors affect the critical position and can occur at the fairlead location or at the bottom of the mooring line[6]. Amaechi et al. (2019) examined the resistance of the CALM riser configuration with a tanker attached to the buoy under different environmental conditions. In this study, the ANSYS AQWA software package was used for the hydrodynamic analysis of the CALM instrument, and the Orcaflex software package was used for riser analysis. The study aimed to determine the effect of flow angle parameters on the behavior of the riser structures, such as curvature, effective tension, and bending moment[7]. Patcher et al. (2014) investigated two types of mooring line configurations, including CALM and SALM methods connected to a wave energy converter, based on the quasi-static analysis. In this study, based on the existing equation for the mooring system, they investigated the effect of the stiffens and size of the mooring lines on the displacement of this structure, as well as its effect on the tension of these mooring lines[8]. Olagnon and Gue'dé (2008) proposed approximate formulae with a combined spectrum of one or several narrow-band LF loads and a higher frequency load based on S-N curves for predicting mooring line fatigue damage. It is

observed that many studies have addressed mooring line fatigue in the literature, but most have focused on chain fatigue in Fairlead[9].

As the literature review above shows, mooring fatigue analysis has traditionally been based on T-N curves, and the most fatigue damage occurs in the Fairlead part. Also, stress amplitudes are calculated based on the tension amplitudes of mooring lines under the combined loading process due to wave frequency (WF) and low frequency (LF) motion. This paper performs T-N curves-based mooring fatigue analyses on a CALM and SALM oil terminal based on conditions of the Persian Gulf region. A comparison is made between CALM and SALM oil terminal-based mooring fatigue analyses and a parametric study is conducted to investigate the impact of K, R, and minimum breaking strength on the fatigue life of mooring lines.

## 2. Governing Equations

In order to identify and compare the structural behavior of these terminals, the governing equations can be of great help in better understanding these oil terminals. In this article, the most important equations governing the problem include diffraction theory, mooring Line and fatigue analysis, which will be explained in detail below.

### 2.1. Diffraction theory

In offshore structure, the theory of diffraction is used as the ratio of the diameter of the structure to the wavelength greater than 0.2 ( $\frac{D}{\lambda} > 0.2$ ) and Morrison equations as the ratio of the diameter of the structure to the wavelength less than 0.2 ( $\frac{D}{\lambda} < 0.2$ ) to calculate the amount of force and the boundary element method is used to discretize the equations. In diffraction theory, the wave force is obtained by calculating the pressure integral on the wet surface of the body[10]. In diffraction theory, the fluid flow field is expressed by the flow potential function, so the potential function must be true in the Laplace equation, and also the boundary conditions must be satisfied with the boundary conditions of the body surface, the boundary conditions of the free surface and the seabed, and the boundary conditions of infinity. Using the principle of superposition of potentials, it can be stated that the total potential arises from three terms for incident wave, diffraction wave, and radiation wave as in Eq. (1). The sum of the potential from the wave and the potential from the wave diffraction is called the Froude-Krylov force.

$$\phi_t = \phi_I + \phi_D + \sum_{R=1}^{R=6} \phi_R \quad (1)$$

in which  $\phi_R$  is the radiation wave potential and  $\phi_D$  is the diffraction wave potential, and  $\phi_I$  (incident wave potential) is the potential of 6 degrees of motion of an

object in static water. By solving the Laplace equation and applying the boundary conditions, we have Eq. (2) as below.

$$\Phi_t = \frac{\zeta_0 g \cosh(h+z)}{\omega \cosh kh} e^{ik(x \cos \theta + y \sin \theta)} \quad (2)$$

in which  $\zeta$  is the amplitude of the collision wave,  $\theta$  is the direction of the wave, and  $K$  is the wave number  $\omega$  of the wave frequency. Potential changes over time are the cause of hydrodynamic forces. As a result, the overall pressure is obtained from Eq. (3).

$$\frac{p}{\rho} = -gz - \frac{\partial \Phi}{\partial t} \quad (3)$$

By considering the Laplace equation, the hydrodynamic pressure will be obtained from Eq. (4).

$$p_h = -i\omega \rho \Phi \quad (4)$$

By integrating the pressure distribution around the wet surface of the structure (diffraction theory), hydrodynamic forces on the body of the structure will be obtained. In this part, all hydrodynamic coefficients such as added mass, damping matrix, and other hydrodynamic characteristics are obtained[11].

## 2.2 Mooring Line

In estimating mooring line forces, the dynamic motion of the mooring line is omitted. The mooring force in each position of the platform is also assumed to be equal to the static force in that position.

For mooring lines that have a zero slope in contact with the seabed as shown in Figure (2), the mooring equations are considered to be in the catenary state, which will be described below.

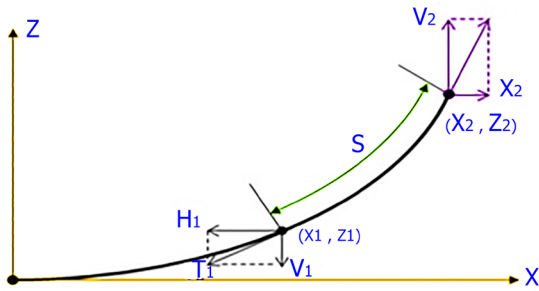


Figure 2. The parameters in the mooring line in the catenary mode[12]

The forces at different points and under different stresses are obtained from Eq. (5) -(9) taking into account the elasticity of the mooring lines. First, the horizontal design load ( $H_2$ ) on the float is calculated based on Eq. (5) and according to other system specifications[8].

$$H_2 = AE \sqrt{\left(\frac{T_2}{AE} + 1\right)^2 - \frac{2WZ_2}{AE}} - A = H \quad (5)$$

in which  $H_2$  is the horizontal design load of the mooring line at the connection to the float,  $AE$  is the axial stiffness of the mooring,  $W$  is the weight of the line,  $T_2$  is the tension created in the mooring line at the upper connection point, and  $Z_2$  is the vertical height of the mooring to the float.

Next, the maximum vertical force, as well as the tension force of the result at the connection point on the float, can be calculated by Eq. (6) and (7).

$$V_2 = WL \quad (6)$$

$$T_2 = \sqrt{H_2^2 + V_2^2} \quad (7)$$

in which  $L$  is the mooring length and  $V_2$  is equal to the vertical design load at the point of connection to the float. By substituting Eq. (7) and (8) in Eq. (5), the obtained horizontal force is rewritten as Eq. (8).

$$H_2 = \frac{V_2^2 - \left(WZ_2 - \frac{W^2 \times L^2}{2 \times AE}\right)^2}{2 \left(WZ_2 - \frac{W^2 \times L^2}{2 \times AE}\right)} \quad (8)$$

Also, the length of the horizontal distance between the beginning and endpoint of the mooring line ( $X_2$ ) can be obtained from Eq. (9).

$$X_2 = \frac{H_2}{W} \sinh^{-1} \left( \frac{WL}{H_2} \right) + \frac{H_2 L}{AE} \quad (9)$$

## 2.3 Fatigue analysis

Fatigue life is estimated by comparing the long-term cyclic loading in a mooring line with its resistance to fatigue damage. For mooring systems, the T-N method is usually used. This method uses the T-N curve, which, based on the test results, provides the number of cycles to failure for a specific mooring component as a function of constant normalized tension range.

The Miner's rule is used to calculate the annual cumulative fatigue damage ratio  $D$  [13] as stated in Eq. (10).

$$D = \frac{n_i}{N_i} \quad (10)$$

in which  $n_i$  is the number of cycles per year in the stress range  $i$  and  $N_i$  is the number of cycles to failure at normalized tension range  $i$  as given by the appropriated T-N curve. The design fatigue life, which is  $1/D$ , must be longer than the useful life in the field multiplied by a safety factor.

The T-N curves presented in Eq. (11) can be used to calculate the fatigue life of the mooring system.

$$NR^M = K \quad (11)$$

in which  $N$  is the number of cycles and  $R$  is the ratio of tension range to reference breaking strength (RBS). If the RBS of a mooring chain is not available, it may be approximately estimated by Eq. (12). Also,  $M$  and  $K$  values are provided in Table 1.

$$RBS(kN) = 0.0211 * d^2(44 - 0.08d) \quad (12)$$

in which  $d$  is the diameter of the mooring chain.

**Table 1. The T-N cure parameters**

Component	M	K
Common stud link	3.0	1000
Common studdles link	3.0	316

The mooring component fatigue design curves are plotted in Figure 3.

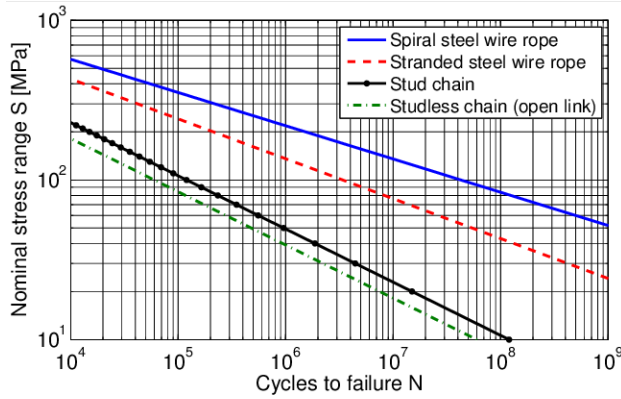


**Figure 3. The mooring fatigue design curves[13]**

The annual fatigue damage, accumulated in a mooring line component as a result of cyclic loading as stated in Eq. (13).

$$D = \sum_{i=1}^n D_i \quad (13)$$

The annual fatigue damage accumulated in an individual state may be computed by Eq. (14).

$$D_i = \frac{n_i}{K} E[R_i^M] \quad (14)$$

in which  $M$  and  $K$  are defined in Table 1,  $n_i$  is the number of tension cycles encountered in state  $i$  per year, and  $E[R_i^M]$  is the mean value of  $R^M$ , which can be expressed by Eq. (15).

$$E(R^M) = \int \left( \frac{2 * T_p}{RBS} \right)^M f(T_p) dT_p \quad (15)$$

For a narrow-banded Gaussian process, peaks of the process,  $T_p$ , follow a Rayleigh distribution, and the probability density function of  $T_p$  is given by Eq. (16).

$$f(T_p) = \frac{T_p}{\sigma^2} e^{\left( \frac{-T_p^2}{2\sigma^2} \right)} \quad (16)$$

in which  $\sigma$  is the standard deviation of the combined LF and WF load process, which can be formulated as Eq. (17).

$$\sigma = \sqrt{\sigma_w^2 + \sigma_l^2} \quad (17)$$

in which  $\sigma_w$  is the standard deviation of the WF tension process and  $\sigma_l$  is the standard deviation of the LF tension process. The zero up-crossing frequency of the combination tension,  $v_{Ci}$ , can be expressed as Eq. (18)-(20).

$$v_{Ci} = \sqrt{\lambda_L v_L^2 + \lambda_W v_W^2} \quad (18)$$

in which

$$\lambda_L = \frac{\sigma_l^2}{\sigma_l^2 + \sigma_w^2} \quad (19)$$

$$\lambda_W = \frac{\sigma_w^2}{\sigma_l^2 + \sigma_w^2} \quad (20)$$

in which  $v_w$  is the zero up-crossing frequency of the wave frequency tension spectrum and  $v_L$  the zero up-crossing frequency of the LF tension spectrum for a sea state.

The number of tension cycles per year in each state can be determined by Eq. (21).

$$n_i = v_i * T_i = v_i * P_i * 3.15576 * 10^7 \quad (21)$$

in which  $v_i$  is the zero up-crossing frequency (hertz) of the tension spectrum in environmental state  $i$ ,  $T_i$  is the time spent in environmental state  $i$  per year, and  $P_i$  is the probability of occurrence of environmental state  $i$ . The expected fatigue damage  $D_i$  for sea state  $i$  can thus be reformulated as Eq. (22) taking into account the T-N curves.

$$D_i = \frac{n_i}{K} (\sqrt{2} \sigma_T)^2 \Gamma(1 + \frac{M}{2}) \quad (22)$$

in which  $\Gamma()$  is the gamma function and  $n_i$  is the number of tension cycles encountered in sea state  $i$ .  $\sigma_T$  is the ratio of the standard deviation of the combined LF and WF tension range to  $RBS$ .

### 3. Methodology

The goal of fatigue analyses of a structure is to ensure that it can withstand exerted cyclic loadings. These loads have a magnitude lower than the resistance of the structures, but their number of occurrences put the structure in a critical condition. The main consequence of these loadings is crack initiation, propagation, and finally sudden failure of the structure.

Due to the cyclic loadings, it is of special importance to study the fatigue analysis of mooring systems of these terminals. Estimating the life of these structures in the same operating and environmental conditions can be effective in selecting the appropriate oil terminal. The fatigue analysis process in these terminals is performed according to Figure 4.

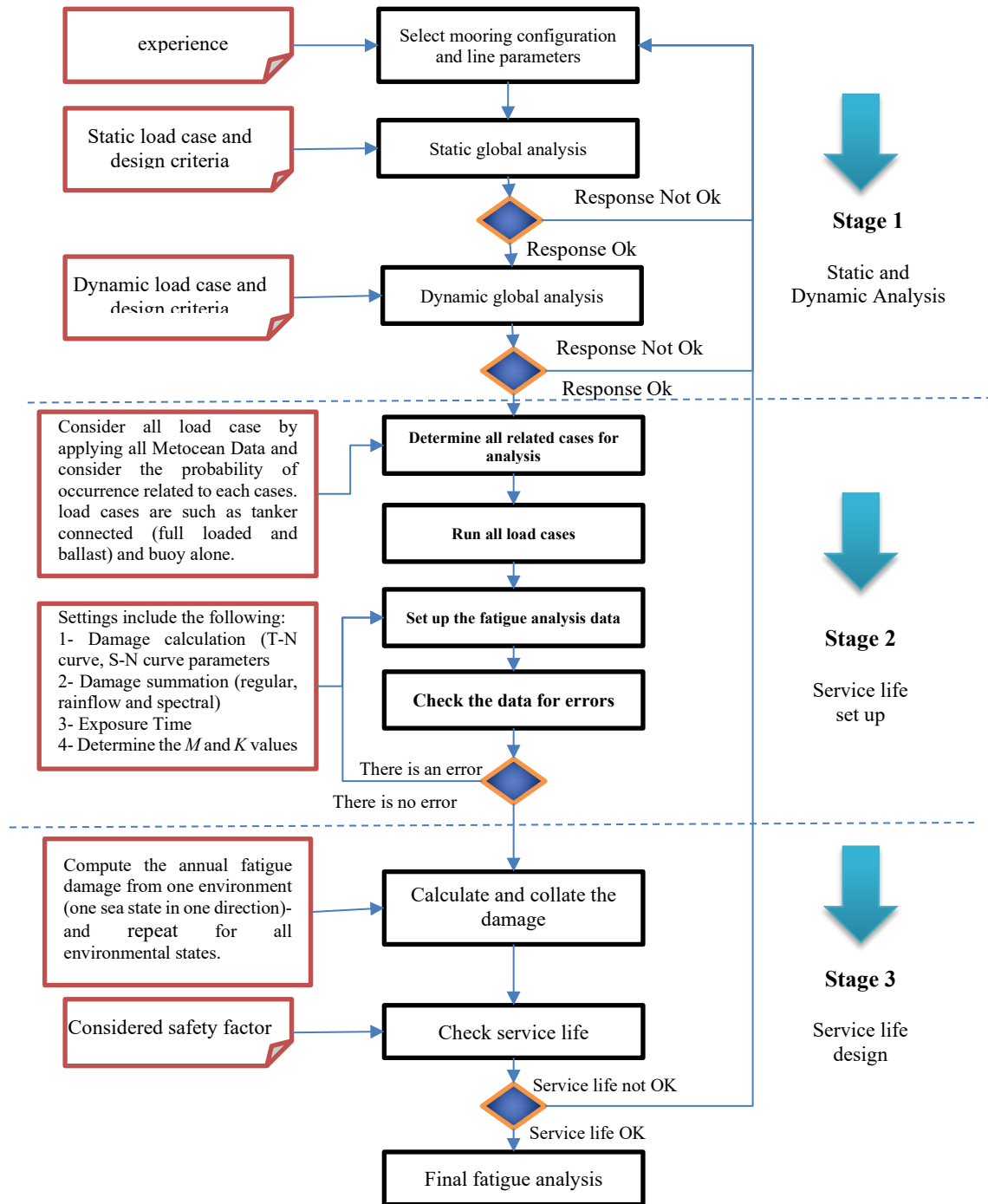


Figure 4. The design process for fatigue analysis-based T-N curve approaches

In stage 1, the mooring configuration is selected based on experience, functional requirements, and material options. After the selection of the configuration system, the static analysis is performed to calculate the pretension in the mooring lines. Also, the unrealistic results are determined by the static analysis. After the static analysis, the dynamic analysis begins in which all the severe load conditions that the structure experiences during its lifetime should be taken into account. For each case, the result must be controlled with role and standard.

Stage 2 involves the primary setup for fatigue design analysis. Before performing a fatigue analysis, we must first prepare a set of simulation files that model

the same system but under different loading conditions that the system will experience over its lifetime. This approach divides sea states that the system will experience into a number of wave classes. This is usually done with a wave scatter table. For each load case, the total time the system is exposed to this load case is named exposure time. Fatigue analysis can be performed with three different types, including regular, rain-flow, or spectral. For both regular and rain flow analyses, each wave class is typically represented with a distinct time-domain simulation. For a regular analysis, the simulation should use a regular wave and for a rain-flow analysis, the simulation should use an irregular wave representative

of the wave class. For a frequency-domain spectral analysis, each wave class should be represented by a distinct frequency domain simulation. These simulations must use an irregular wave representative of the wave class. This paper uses the rain-flow fatigue analysis as it is the most accurate method.

In stage 3, the analysis begins in which the damage is then collated and summed for specified load cases and is then presented either as plots or in tabular fashion. In this stage, the predicted mooring component fatigue life shall be at least three times as long as the design service life of the mooring system.

Then, the fatigue life of each oil terminal is calculated and compared in terms of the mooring line. The sensitivity of their design life to various parameters is also investigated.

#### 4. Modeling

The finite element model includes vessels, mooring lines, and the interaction of these two components. In the finite element analysis considered in this paper, the impact of vessels including the tanker and buoys of the

terminal is considered as boundary conditions for mooring lines in each stage of dynamic analysis.

In this regard, a coupled analysis is performed for the buoys and tanker to investigate the response caused by both floating motion and hydrodynamic loads. In this paper, the floating body is first modeled in Maxsurf software. Then, to obtain hydrodynamic and hydrostatic coefficients, the floating body is transferred to Ansys Aqwa software. Diffraction/radiation simulation is performed using Ansys Aqwa to obtain hydrodynamic data for the buoys and tankers. At this stage, the geometry of the buoys, as well as their mass characteristics and amount of draft, are adjusted. The hydrodynamic data obtained in the previous step, including RAO and quadratic transfer functions (QTF), are imported into Orcaflex software. The outputs are then transferred to Orcaflex software to perform a fatigue analysis for the mooring line after creating a coupled model of the tanker and the terminal. The design process in the software is illustrated in Figure 5.

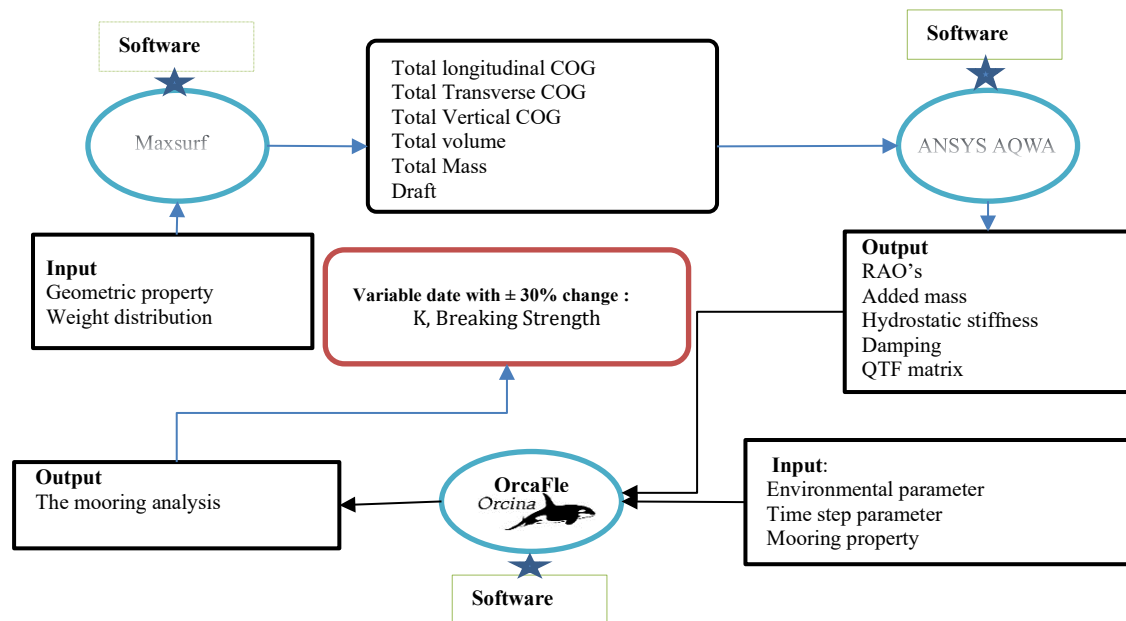


Figure 5. The design process for modeling the oil terminal in the software

The hydrodynamic model of the buoys and tanker created at Ansys Aqwa is shown in Figure 6.

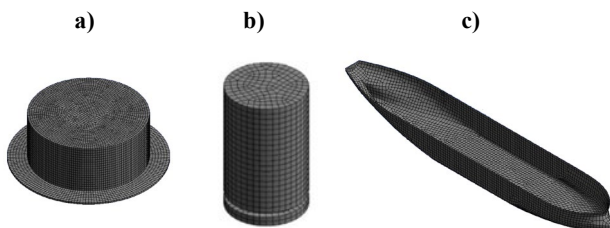


Figure 6. The models made in Ansys Aqwa software for a) CALM, b) SALM, and c) oil tanker

The first step in the analysis and design process is to determine the load and forces on the studied structures. The forces acting on these structures include forces from waves, winds, and currents. Wind and current loads are determined using the OCIMF standard. Also, the interaction between wave loads and vessels can be divided into three load types, including first-order wave loads, second-order wave loads, and also second-order loads with wind oscillating loads that lead to an LF motion. First-wave motions are defined as wave frequency motions that can be calculated by RAO. Second-order forces, defined as wave drift forces, are also identified by

QTF inputs. The LF motion of vessels controlled by the resonance phenomenon dominates their natural frequency. The range of motion depends very much on the stiffness of the mooring system and the damping of the system. Accurate estimation of system attenuation is very important when calculating low frequency. The main sources of damping include wave drift and mooring system.

OrcaFlex uses a finite element for a mooring line as shown in Figure 7. This line is divided into a series of line segments that are then modeled by the massless model segments with a node at each end. Each segment is a straight massless element that models the axial and torsional properties of structural components. Other properties, such as mass and buoyancy, all focus on nodes[14].

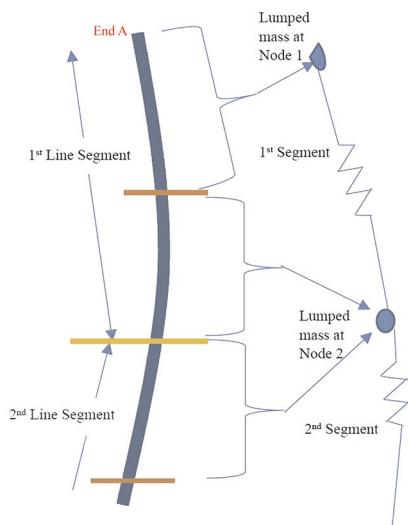


Figure 7. The OrcaFlex line model

#### 4.1 Mesh independence

To check the convergence of the mesh, the size of the elements should be fine-tuned in the selected areas and the desired outputs should be checked. According to the values in Table 2, to investigate the independence of the mesh (for CALM buoy), the response amplitude operator (RAO) in Heave motion is shown for different sizes of mesh elements.

Table 2. The specifications of mesh independence for heave motion

Case	1	2	3	4	5	6
Max. mesh size(m)	2	0.8	0.4	0.2	0.1	.05
Number of elements	408	2292	8850	33080	128902	450125

As is clear in Figure 8, from case 4 onwards, the response amplitude operator in Heave motion has not changed much. Therefore, the size of the mesh element is considered to be 0.2.

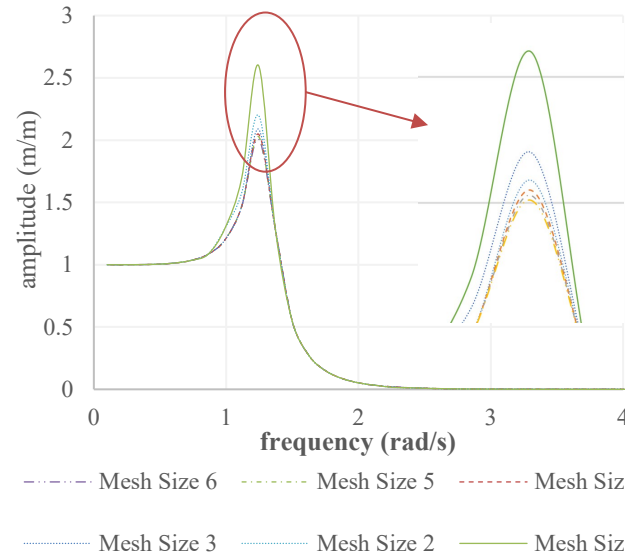
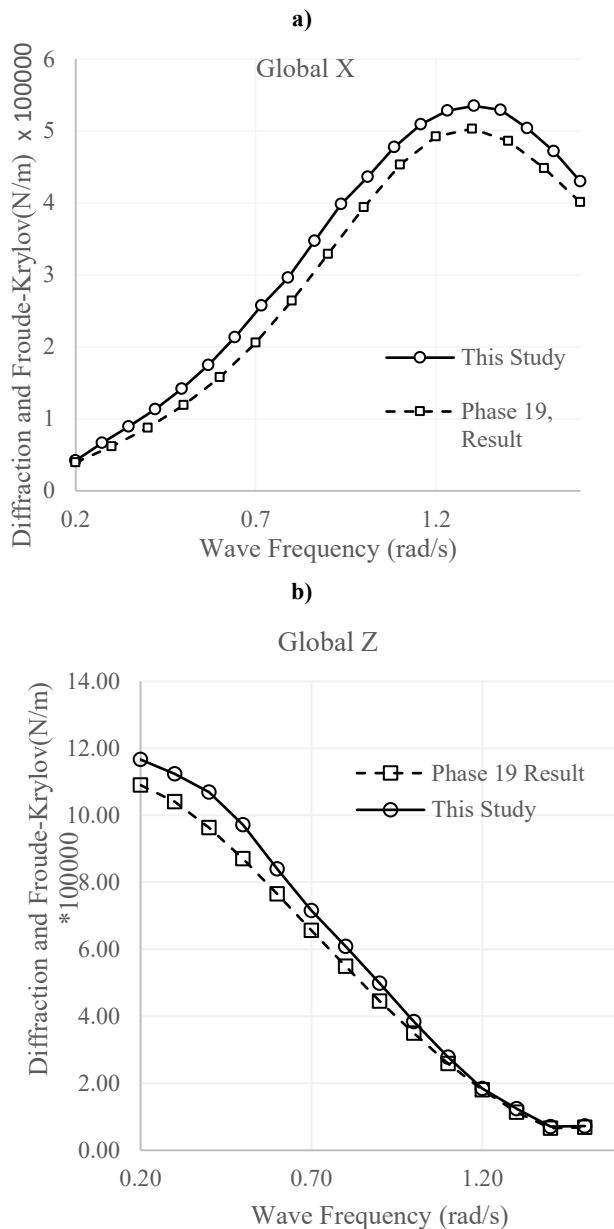


Figure 8. The response amplitude operator in Heave motion for different mesh element sizes

#### 4.2 Model verification

To ensure the validity of the model, the results are compared with the CALM modeled in the Persian Gulf region. This paper compares the load RAO results for the CALM buoy in the X and Z directions in Fig. 9 and Table 3.



**Figure 9. The comparison of load RAO results for a CALM buoy with the results of a CALM buoy designed in the Persian Gulf region; a) X direction, b) Z direction**

**Table 3. Comparison Result between Phase 19 and this study, Diffraction and Froude-Krylov (KN/m)**

f rad/s	Global X			Global Z		
	Phase 19	This Study	Error %	Phase 19	This Study	Error %
0.2	3.95 E+01	4.21 E+01	<b>6.62</b>	1.09 E+03	1.17 E+03	<b>7.00</b>
0.4	8.74 E+01	9.04 E+01	<b>3.54</b>	1.04 E+03	1.12 E+03	<b>11.00</b>
0.6	1.58 E+02	1.73 E+02	<b>9.69</b>	9.63 E+02	1.07 E+03	<b>9.80</b>
0.8	2.64 E+02	2.96 E+02	<b>12.1</b> <b>9</b>	8.70 E+02	9.72 E+02	<b>10.80</b>
1	3.94 E+02	4.36 E+02	<b>10.6</b> <b>9</b>	7.65 E+02	8.40 E+02	<b>10.00</b>
1.2	4.92 E+02	5.28 E+02	<b>7.38</b>	6.56 E+02	7.15 E+02	<b>2.10</b>
1.4	4.86 E+02	5.29 E+02	<b>8.89</b>	5.49 E+02	6.08 E+02	<b>7.41</b>
1.6	4.01 E+02	4.30 E+02	<b>7.23</b>	4.45 E+02	4.98 E+02	<b>5.42</b>

According to Figure 9, it can be said that the model shows a good agreement with the result of CALM designed in the Persian Gulf region. In the verification performed, the load RAO has been investigated at different frequencies and directions. The studied structure is a CALM buoy its diameter and height are 12.5 and 5.3 meters, respectively. The slight difference between the results is due to the insufficient data on the details of the reference model.

Figure 10 shows a model of a moored tanker by two common mooring terminals in Orcaflex software. As shown in Figure 10-a, the CALM structure is anchored to the seabed by six mooring chains 380 m long. The body of this terminal consists of two parts that are connected by a joint so that if the tanker rotates, the upper part of the terminal will also rotate. The CALM terminal in operation is usually connected to the tanker by two hawsers. As shown in Figure 10-b, the SALM terminal is anchored to the seabed by 38.8 m long mooring (proportional to the water depth in the study area) and the tanker is secured by its two hawsers. This type of structure makes the buoy rotatable due to the type of chain connections, which is a universal connection.

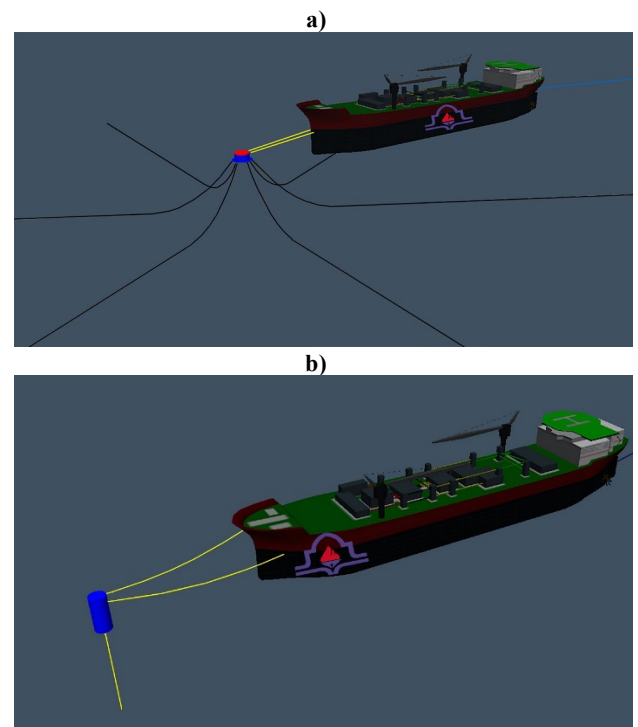


**Figure 10. Modeling of the types of terminals studied in Orcaflex software; a) CALM, b) SALM**

## 5. Case Study

Specifications of CALM structure according to the terminal built in the Persian Gulf region, and for the SALM terminal according to the structure built in the Gulf of Mexico, due to the same tonnage of tankers and also the same environmental conditions for two oil terminals have been selected. The mechanical

specifications of each of these terminals and the environmental conditions are mentioned below.

### 5.1. Vessels

The geometric characteristics and effective parameters used in modeling the floating oil terminals and tankers studied in this paper are presented in Table 4. To compare the effect of offshore terminal type on the response of transport system structures, the paper calculates the characteristics of the CALM structure according to the actual sample of the terminal built in the Persian Gulf and the characteristics of the SALM structure according to the structure built in the Gulf of

Mexico for the highest tonnage of the tanker connected to it. The metacentric height is considered a criterion for evaluating the stability of the modeled buoys.

For all these buoys, this parameter is greater than one, so both terminals will be stable. The buoy of the CALM terminal is composed of two components connected by a joint so that if the tanker rotates, the upper part of the terminal will also rotate. A schematic view of the buoys is shown in Figure 11.

**Table 4. The specifications of the vessels modeled in the study**

Parameters	Unit	CALM	SALM	Tanker
		Value		
Draft	m	3.266	9	22.6
Center of gravity (X-direction)	m	0	0	170.18
Center of gravity (Y-direction)	m	0	0	0
Center of gravity (Z-direction)	m	-0.766	6	17.3
Moment of inertia(X-direction)	$kg \cdot m^2$	484E+4	624.4E+4	8.260E+10
Moment of inertia(X-direction)	$kg \cdot m^2$	484E+4	624.4E+4	2.35E+12
Moment of inertia(X-direction)	$kg \cdot m^2$	935E+4	289E+4	2.35E+12
Diameter	m	12.5	6.4	-
Diameter of skirt	m	16.63	-	-
Weight	ton	289.98	400	-
Height	m	5.3	14	-
Length between perpendicular, $L_{BP}$	[m]	-	-	320
Breadth molded, B	[m]	-	-	60
Depth, D	[m]	-	-	30.5
Windage area, $A_L$ (longitudinal), surge area	[m <sup>2</sup> ]	29.53	32	1155.25
Windage area, $A_T$ (Transverse), sway area	[m <sup>2</sup> ]	29.53	32	3693.81
Windage area, $A_T \cdot L_{BP}$ , yaw area	[m <sup>3</sup> ]	369.12	204.8	1.182E6
Displacement	[kg]	-	-	3.6712E+08

### 5.2 Mooring line

To moor the buoy of the CALM terminal on the seabed, six moorings made of studless chains are modeled as linear elastics and their bending and torsional effects are assumed to be negligible. Each of these chains with a length of 380 meters is placed in a circular position on the periphery of the sea. The  $C_d$  and  $C_M$  coefficients are considered constant for all mooring lines during the analysis and the amount of pretension in each morning is equal. In the SALM terminal, a stud mooring is used to control the buoy. This type of structure also makes the buoy rotatable due to the type of chain connection, which is a universal connection. To simulate this feature in Orcaflex software for two ends of the mooring, one in the seabed and the other connected to the buoy, zero bending stiffness and torsion are considered, which allows free rotation at both ends of the mooring. General specifications and parameters required for the modeling of the mooring are given in Table 5.

**Table 5. The specifications of the mooring line.**

Parameters	Unit	Value	
		CALM	SALM
Diameter	mm	95	175
Length	m	380	38.8
Weight	Kg/m	180	671
Axial stiffness	kN	712000	3093000
Minimum breaking load	kN	8180	25173
$C_d$	-	1.2	1.2
$C_M$	-	1	1

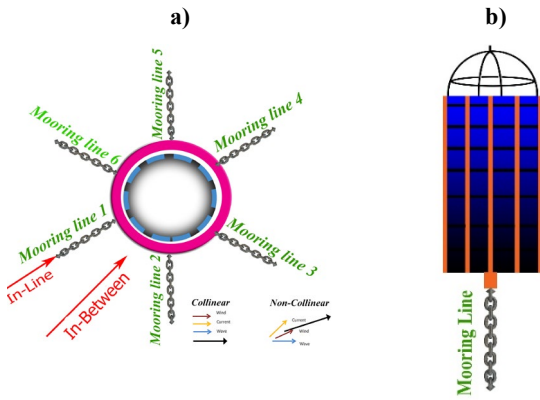


Figure 11. The arrangement of the mooring line; a) CALM system, b) SALM system

In this study, to connect the tanker to the terminal, two hawsers are used for each terminal buoy, which is nonlinearly modeled in Figure 12. The length of these hawsers is 60.96 m and their maximum allowable tension (MBL) is 5800 kN

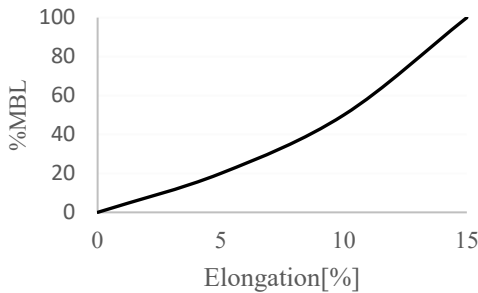


Figure 12. The non-linear axial stiffness in the hawser system.

### 5.3 Environmental Condition

The forces acting on these structures include forces from waves, winds, and currents. A combination of these forces also has a significant impact on the total incoming forces. Due to the wave phenomenon, two important forces of drag and inertia are created on the structure so that all the forces created by the wave are the result of these two forces. The drag force of  $F_D$  is affected by the velocity of the fluid, which depends on the shape and roughness of the body, the Reynolds number, and the intensity of the turbulence in the flow. The inertial force  $F_I$  is caused by the acceleration of the fluid particles (water).

Morrison equation is used to calculate the wave force in slender components, such as mooring and risers, and diffraction theory is used for components whose body dimensions are larger than the wavelength, such as vessels. The transverse and rotational displacements in the vessel are calculated by RAO using Eq. (23) for each wave height and period.

$$X = A \cdot RAO \cdot \cos(\omega t + \psi) \quad (23)$$

in which  $X$  is the response of the structure,  $A$  is the amplitude of the wave,  $\Psi$  and  $\omega$  are the angles of the frequency flow and the frequency of the wave,

respectively. Due to the windage surface of the upper part of the tanker, the wind force is of great importance. This force is due to the change in pressure created in the free wind flow and is a function of wind speed, direction, surface, and shape of structural members.

According to the study area, the wave spectrum used in this study is the modified Jonswap spectrum that is appropriate to the environmental conditions of the Persian Gulf. It is presented in Eq. (24).

$$S(\omega) = \frac{\alpha g^2 \gamma^\alpha}{\omega^5} \exp\left(-\frac{5}{4} \frac{\omega_p^4}{\omega^4}\right) \quad (24)$$

in which  $g$  is a gravitational constant, and the key parameters for defining this spectrum include the characteristic wave height  $H_s$ , spectral peak period  $T_p$ , and the peak enhancement factor  $\gamma$ , which are presented in Table 5 for this study. To compare the terminals in the same conditions, a wave direction of 30 degrees relative to the direction of the tanker is considered. Also, the direction of the wind force and current is parallel to the wave force.

The sea conditions of the Persian Gulf region considering wave, wind, and current in collinear directions are listed in Table 6. For the fatigue analysis, the wind and current speed are selected based on the 95% probability of occurrence.

**Table 5. Metocean Data for Fatigue Analysis**

NO.	H <sub>s</sub> [m]	T <sub>z</sub> [s]	$\gamma$	Wind(m/s)	Current(m/s)	Probability		
						Ballast	Full Loaded	Stand Alone
1	0.25	0.5	1.4933	16.14	0.2445	6.83E-04	6.83E-04	2.73E-03
2	0.25	1.5	1.4933	16.14	0.2445	4.57E-03	4.57E-03	1.83E-02
3	0.25	2.5	1.4933	16.14	0.2445	1.35E-02	1.35E-02	5.39E-02
4	0.25	3.5	1.4933	16.14	0.2445	2.42E-02	2.42E-02	9.67E-02
5	0.25	4.5	1.4933	16.14	0.2445	7.85E-03	7.85E-03	3.14E-02
6	0.25	5.5	1.4933	16.14	0.2445	6.33E-04	6.33E-04	2.53E-03
7	0.25	6.5	1.4933	16.14	0.2445	8.33E-05	8.33E-05	3.33E-04
8	0.5	3.5	1.4933	16.14	0.2445	2.84E-02	2.84E-02	1.13E-01
9	0.5	4.5	1.4933	16.14	0.2445	1.87E-02	1.87E-02	7.47E-02
10	0.5	5.5	1.4933	16.14	0.2445	5.37E-03	5.37E-03	2.15E-02
11	0.5	6.5	1.4933	16.14	0.2445	1.27E-03	1.27E-03	5.07E-03
12	0.5	7.5	1.4933	16.14	0.2445	5.00E-05	5.00E-05	2.00E-04
13	0.75	3.5	1.4933	16.14	0.2445	8.62E-03	8.62E-03	3.45E-02
14	0.75	4.5	1.4933	16.14	0.2445	1.49E-02	1.49E-02	5.95E-02
15	0.75	5.5	1.4933	16.14	0.2445	4.78E-03	4.78E-03	1.91E-02
16	0.75	6.5	1.4933	16.14	0.2445	2.82E-03	2.82E-03	1.13E-02
17	0.75	7.5	1.4933	16.14	0.2445	8.33E-05	8.33E-05	3.33E-04
18	0.75	8.5	1.4933	16.14	0.2445	2.10E-03	2.10E-03	8.40E-03
19	1	3.5	1.4933	16.14	0.2445	6.08E-03	6.08E-03	2.43E-02
20	1	4.5	1.4933	16.14	0.2445	6.15E-03	6.15E-03	2.46E-02
21	1	5.5	1.4933	16.14	0.2445	6.15E-03	6.15E-03	9.53E-03
22	1	6.5	1.4933	16.14	0.2445	1.67E-04	1.67E-04	6.67E-04
23	1	7.5	1.4933	16.14	0.2445	1.67E-05	1.67E-05	6.67E-05
24	1.25	3.5	1.4933	16.14	0.2445	2.83E-04	2.83E-04	1.13E-03
25	1.25	4.5	1.4933	16.14	0.2445	1.62E-03	1.62E-03	6.47E-03
26	1.25	5.5	1.4933	16.14	0.2445	3.57E-03	3.57E-03	1.43E-02
27	1.25	6.5	1.4933	16.14	0.2445	2.37E-03	2.37E-03	9.47E-03
28	1.25	7.5	1.4933	16.14	0.2445	2.33E-04	2.33E-04	9.33E-04
29	1.25	8.5	1.4933	16.14	0.2445	3.33E-05	3.33E-05	1.33E-04
30	1.5	4.5	1.4933	16.14	0.2445	2.67E-04	2.67E-04	1.07E-03
31	1.5	5.5	1.4933	16.14	0.2445	9.33E-04	9.33E-04	3.73E-03
32	1.5	6.5	1.4933	16.14	0.2445	1.85E-03	1.85E-03	7.40E-03
33	1.5	7.5	1.4933	16.14	0.2445	2.50E-04	2.50E-04	1.00E-03
34	1.5	8.5	1.4933	16.14	0.2445	3.33E-05	3.33E-05	1.33E-04
35	1.75	4.5	1.4933	16.14	0.2445	1.67E-05	1.67E-05	6.67E-05
36	1.75	5.5	1.4933	16.14	0.2445	1.00E-04	1.00E-04	4.00E-04
37	1.75	6.5	1.4933	16.14	0.2445	9.33E-04	9.33E-04	3.73E-03
38	1.75	7.5	1.4933	16.14	0.2445	2.33E-04	2.33E-04	9.33E-04
39	1.75	8.5	1.4933	16.14	0.2445	5.00E-05	5.00E-05	2.00E-04
40	2	6.5	1.4933	16.14	0.2445	2.67E-04	2.67E-04	1.07E-03
41	2	7.5	1.4933	16.14	0.2445	1.83E-04	1.83E-04	7.33E-04
42	2	8.5	1.4933	16.14	0.2445	6.67E-05	6.67E-05	2.67E-04
43	2.25	6.5	1.4933	16.14	0.2445	5.00E-05	5.00E-05	2.00E-04
44	2.25	7.5	1.4933	16.14	0.2445	8.33E-05	8.33E-05	3.33E-04
45	2.25	8.5	1.4933	16.14	0.2445	3.33E-05	3.33E-05	1.33E-04
46	2.5	7.5	1.4933	16.14	0.2445	1.67E-05	1.67E-05	6.67E-05

## 6. Results

In this paper, the mooring systems of two common oil terminal models are subjected to fatigue analysis, and the effective parameters in the governing relations are subjected to sensitivity analysis. Effective parameters in the existing relationships including the  $K$  value, the ratio of tension range to reference breaking strength  $R$ ,

and the effect of the weight of the tanker are examined in two tonnages (including ballast and full-loaded). Since one of the most important parameters is the value of  $R$ , so in the mooring line of the CALM and SALM oil terminals, the value of  $R$  is compared in the worst possible case. The results of this section are shown in Figure 13.

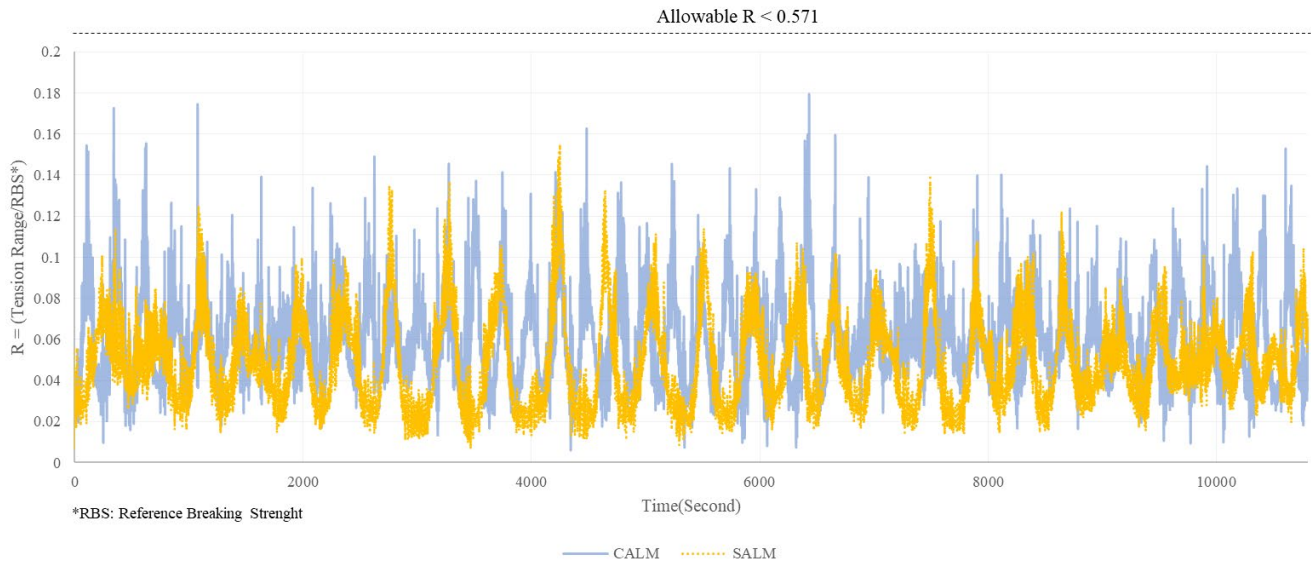


Figure 13: The comparison of  $R$  ratio in the CALM and SALM terminal according to the worst case of loading

Based on the results, the  $R$ -value in the CALM terminal shows a higher value than that in the SALM terminal at different times so that the maximum value is 0.17 for the CALM terminal and 0.15 for the SALM terminal.

The design life of the CALM and SALM mooring lines, given the same conditions, will help us to know more about these terminals and better compare them. Figure 14 shows the design life of these two terminals.

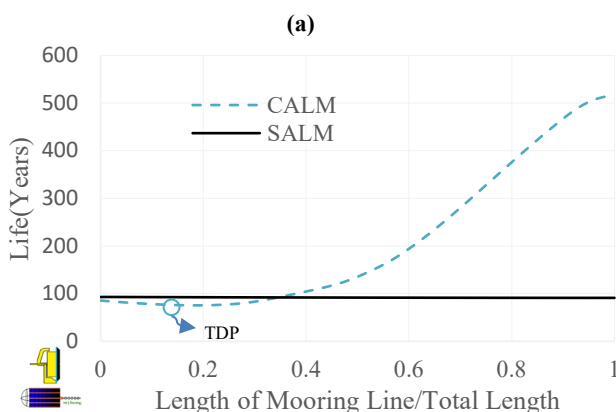


Figure 14: The design life of the mooring system according to all relevant load cases for CALM and SALM oil terminal

The results show that the design life of the SALM mooring line will be longer than that of the CALM mooring. The minimum design life of the SALM mooring is 91 years while it is 75 years for the CALM

terminal. It can also be seen that the most critical point for the design life is the connection point of the mooring line to the seabed in the SALM terminal and the location of the mooring line on the seabed (TDP) in the CALM terminal.

Most of the damage that occurs in the mooring system is the result of two load cases, including a fully-loaded tanker and a ballast tanker. Figure 15 illustrates the amount of fatigue caused by each load case.

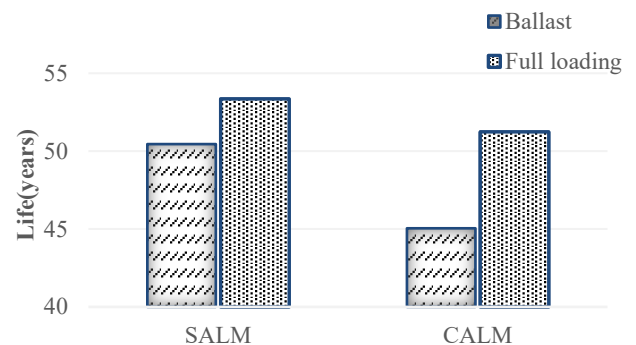


Figure 15: The effect of the tonnage (draft) of the tanker on mooring life

The results show that in the CALM terminal, the difference in fatigue caused by the two load cases, including ballast and full-load, shows more. This difference is due to the large amount of tension force created in the ballast state. At the SALM terminal, the

fatigue caused by the two load cases shows less difference.

There are two important parameters in the fatigue equations. These parameters include the amount of  $K$  and the amount of  $R$ . Therefore, the examination of the effect of these parameters on fatigue has a significant effect on recognizing these parameters. In this paper, the amount of fatigue created in the mooring system of the two terminals of CALM and SALM with a 30% change in the amount of parameters  $K$  and  $R$  are done, and the results are included in Figures 16 and 17.

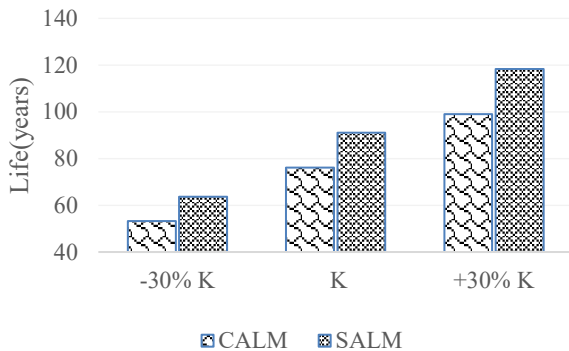


Figure 16: The effect of the  $K$  value on mooring life

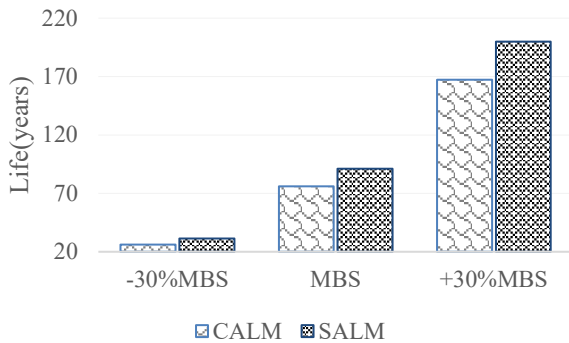


Figure 17: The effect of  $MBS$  on mooring life

The results show that when the parameters are changed, fatigue in both CALM and SALM terminals change similarly. It is also observed that with a change in the  $MBS$  parameter, the fatigue life changes to a greater extent.

## 7. Conclusion

In this paper, the mooring system of two common oil terminals is subjected to fatigue analysis according to the S-N curve approach and the fatigue life of their mooring systems is compared with each other. Also, the sensitivity analysis of its important parameters, including the value of  $K$  and the value of  $R$ , is discussed. The most important results can be summarized as below.

Under the same environmental conditions with the same tanker tonnage, the fatigue life of the SALM terminal mooring system shows a greater fatigue life.

- One of the most effective parameters to check the fatigue rate of the mooring system based on the S-N curve is the  $R$  ratio. The results show that in all cases, the value of  $R$  in the mooring line of the SALM terminal, although more tension is generated, the ratio of  $R$  is less and will improve the life of fatigue.
- When calculating the fatigue life, the most fatigue damage occurs in both floating terminals when the ballast tanker is connected.
- Other effective parameters are  $MBS$  and  $K$  values. According to the sensitivity analysis, it is observed that by changing the value of  $MBS$ , the fatigue life of the CALM and SALM terminals changes by 119% and 100%, respectively. It is also observed that by changing the amount of  $K$  value, the fatigue life of the CALM and SALM terminals changes by the same amount.

## 8. References

- [1] Wichers, J., (2013) *Guide to single point moorings*. WMooring.
- [2] Gruy R. H. and et al, (1979), *The LOOP deepwater port: Design and construction of the Single Anchor Leg Mooring (SALM) tanker terminals*, in Proceedings of the Annual Offshore Technology Conference, vol. 1979-May, pp. 1793–1803.
- [3] Xue, X. and et al, (2018), *Mooring system fatigue analysis for a semi-submersible*, Ocean Eng., vol. 156, pp. 550–563.
- [4] Laval G. de, (1971), *Fatigue tests on anchor chain-cable*, in Offshore Technology Conference.
- [5] Olsen M. K., (2011), *Estimation of annual probability of mooring line failure as a function of safety factors*, Norges teknisk-naturvitenskapelige universitet, Fakultet for .
- [6] Wu, Y. and Wang, T., (2015), *Governing factors and locations of fatigue damage on mooring lines of floating structures*, Ocean Eng., vol. 96, pp. 109–124,.
- [7] Amaechi, C. V., Wang, F., Hou, X., and Ye, J., (2019) *Strength of submarine hoses in Chinese-lantern configuration from hydrodynamic loads on CALM buoy*. Ocean Eng., vol. 171, pp. 429–442.

- [8] Pecher, A., Foglia, A., and Kofoed, J. P., (2014), *Comparison and sensitivity investigations of a CALM and SALM Type mooring system for wave energy converters*, J. Mar. Sci. Eng., vol. 2, no. 1, pp. 93–122, Feb..
- [9] Olagnon, M. and Guede, Z., (2008) , *Rainflow fatigue analysis for loads with multimodal power spectral densities*, Mar. Struct., vol. 21, no. 2–3, pp. 160–176,.
- [10] D. N. Veritas, “DNV-RP-C205, (2010) *Environ. Cond. Environ. loads*.
- [11] Tafazzoli, S. and Shafaghat, R., (2019) ,*Investigating the behavior of the mooring system for a conceptual design of a spar floating wind turbine under survival conditions*, J. Mar. Eng., vol. 15, no. 29, pp. 49–62.
- [12] “AQWA User Manual.” [Online]. Available: [https://www.sharcnet.ca/Software/Ansys/14.0/en-us/help/wb\\_aqwa/wb\\_aqwa.html](https://www.sharcnet.ca/Software/Ansys/14.0/en-us/help/wb_aqwa/wb_aqwa.html). [Accessed: 19-Sep-2018].
- [13] API, *API RP2SK.Design and analysis of stationkeeping systems for floating structures*,(2015), 3rd ed. American Petroleum Institute.
- [14] Orcaflex, *OrcaFlex Manual version 9.7a,2015*. section 1;3;4;6;7, 2015.